ACS APPLIED MATERIALS & INTERFACES

Research Article

www.acsami.org

Exploring the Segregating and Mineralization-Inducing Capacities of Cationic Hydrophilic Polymers for Preparation of Robust, Multifunctional Mesoporous Hybrid Microcapsules

Jiafu Shi, Wenyan Zhang, Xiaoli Wang, Zhongyi Jiang,* Shaohua Zhang, Xiaoman Zhang, Chunhong Zhang, Xiaokai Song, and Qinghong Ai

Key Laboratory for Green Chemical Technology of Ministry of Education, School of Chemical Engineering and Technology, Tianjin University, Tianjin 300072, China

Supporting Information

ABSTRACT: A facile approach to preparing mesoporous hybrid microcapsules is developed by exploring the segregating and mineralization-inducing capacities of cationic hydrophilic polymer. The preparation process contains four steps: segregation of cationic hydrophilic polymer during template formation, cross-linking of the segregated polymer, biomimetic mineralization within cross-linked polymer network, and removal of template to simultaneously generate capsule lumen and mesopores on the capsule wall. Poly(allylamine hydrochloride) (PAH) is chosen as the model polymer, its hydrophilicity renders the segregating capacity and spontaneous enrichment in the near-surface region of $CaCO_3$ microspheres; its biopolyamine-mimic structure renders the mineralization-inducing capacity to produce titania from the water-soluble titanium(IV) precursor. Meanwhile, $CaCO_3$ microspheres serve the dual templating functions in the formation of hollow lumen and mesoporous wall. The thickness of capsule wall can be controlled by changing the polymer segregating and cross-linking conditions, while the pore size on the capsule wall can be tuned by changing the template synthesizing conditions. The robust hybrid microcapsules exhibit desirable efficiency in enzymatic catalysis, wastewater treatment and drug delivery. This approach may open facile, generic, and efficient pathway to designing and preparing a variety of hybrid microcapsules with high and tunable permeability, good stability and multiple functionalities for a broad range of applications.

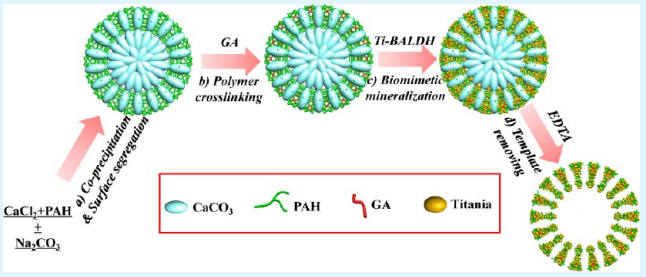

KEYWORDS: *mesoporous hybrid microcapsules, surface segregation, biomimetic mineralization, templating, multifunctionalities*

1. INTRODUCTION

In nature, cell demonstrates an exceptional archetype of microencapsulation and compartmentation, for either protecting the encapsulated substances from leakage/environmental attacks or controlling the selective transport/release/uptake of the substances out/into the cell. By virtue of this configuration, cell manipulates the chemical reactions and equilibria in quite an efficient manner.[1] As a mimic of cell, synthetic microcapsule has been attracted intense research and development interest because of its unique and hierarchical structure. However, to the best of our knowledge, majority of studies focus on the capsule lumen and the capsule wall, seldom dealt with the pores on the capsule wall.[2]

Since the discovery of the novel family of molecular sieves called M41S,[3] research on mesoporous materials has experienced an astonishing increase in the past twenty years. Theoretically, mesopores with the pore size ranging from 2 to 15 nm are of peculiar significance for a broad spectrum of emerging applications which involve large guest molecules and require fine-tuning of guest binding, release, or diffusion (e.g., separation, catalysis, drug delivery, etc.).[4] It can be envisaged that mesopores on a capsule wall will provide the accessible channels for the transportation of small molecules with low mass transfer resistance. Meanwhile, the mesopores can control the permeability of the capsule wall for the exchange of large-sized molecules between the capsule lumen and the outer environment. Therefore, mesoporous microcapsules with tunable pore size, high porosity, large specific surface area and surface muliti-functionalities are of great demand.

When designing an approach for the preparation of mesoporous microcapsules, the following three critical structural/morphological characteristics should be taken into consideration: (1) the size and shape of the entire microcapsule, as well as the lumen of the microcapsule; (2) the thickness, structure/morphology, and the stability of the capsule wall; and (3) the pore size and porosity on the capsule wall.[5] Compared with the former two issues, the latter one is far less exploited. In general, the existing approaches to mesoporous microcapsules can be fallen into two categories based on the templates for the formation of hollow interiors,

Received: March 19, 2013
Accepted: May 15, 2013
Published: May 15, 2013

   dx.doi.org/10.1021/am401017y | ACS Appl. Mater. Interfaces 2013, 5, 5174−5185

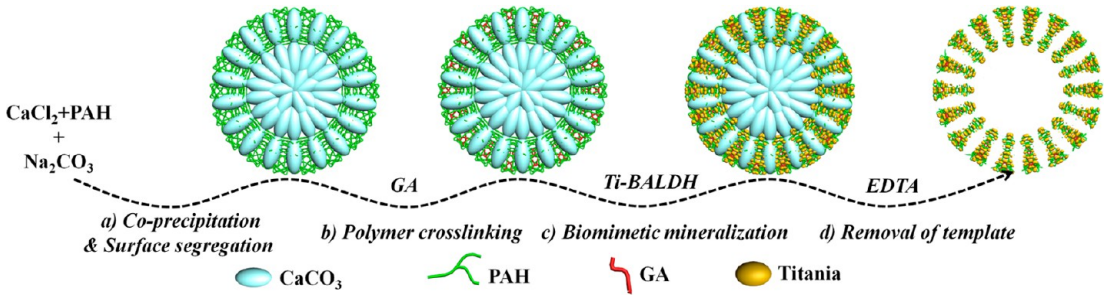

Figure 1. Schematic preparation procedure of PGTi microcapsules: (a) formation of P-$CaCO_3$ microspheres through coprecipitation of PAH-containing $CaCl_2$ and Na_2CO_3 accompany with surface segregation of PAH; (b) formation of PG-$CaCO_3$ microspheres through cross-linking of PAH via GA; (c) formation of PGTi-$CaCO_3$ microspheres through biomimetic mineralization induced by cross-linked PAH network; and (d) formation of PGTi microcapsules after removing $CaCO_3$ microsphere via EDTA treatment.

soft templating approach and hard templating approach.[5] In comparison, hard templates, such as polymer latices, inorganic oxides, and salts,[2a,6] are more effective in synthesizing mesoporous microcapsules with well-defined size and morphology as a result of the desirable stability and monodispersity of the templates. For the current hard templating method, the templates only contribute to formation of the capsule lumen since the capsule wall grows outward from the surface of the templates. To acquire mesopores on the capsule wall, the pore-forming agents have to be incorporated.[2a] For instance, a variety of surfactants have been utilized as pore forming agents for the preparation of inorganic mesoporous microcapsules. However, these surfactants can only be removed through hydrothermal treatment, calcination, or solvent extraction. Similarly, during the synthesis of organic mesoporous microcapsules, inorganic nanoparticles (mainly silica nanoparticles) are utilized as pore-forming agents, which can only be etched by hydrofluoric acid or alkali treatment. Apparently, these operations make the synthesis procedure complicated and harsh.[7] In the past decades, polyelectrolyte mesoporous microcapsules have been sporadically synthesized through layer-by-layer (LbL) self-assembly.[8] The mesopores could be generated by varying the assembly number of polyelectrolyte layers without adding pore-forming agents. Nevertheless, there exists a pronounced trade-off effect between the pore size/porosity and the mechanical strength of the microcapsules.[9] Therefore, developing a facile, mild and controlled approach to robust, mesoporous microcapsules is urgently desired.

Incorporating rigid inorganic blocks into flexible organic microcapsules has been proven to be able to enhance the mechanical strength because of the existence of numerous hydrogen, van der Waals, or ionic bonds between organic and inorganic blocks.[10] Moreover, hybridization could offer new opportunities to create materials with multifunctional properties. In recent years, biomimetic mineralization, as a novel, green, and efficient platform technique for hybrid materials synthesis, has been delicately implanted to prepare various robust organic−inorganic hybrid microcapsules.[10b,11] For instance, Yang et al.[11] have conducted silica encapsulation of individual yeast cells through alternate LbL self-assembly of polycations and polyanions onto the surface of yeast cells and the subsequent biomimetic silicification. Significantly enhanced cell viability is acquired. Very recently, a variety of hybrid microcapsules with controlled structure/morphology and high mechanical strength have been fabricated in our group using biomimetic mineralization approaches.[10c,d] Nevertheless, these preparations were all conducted in an open space, therefore, the formation of pores on the capsule wall was not the major concern.

In the present study, a kind of mesoporous hybrid microcapsules has been synthesized by exploring the segregating and mineralization-inducing capacities of cationic hydrophilic polymers as shown in Figure 1. One distinct feature is that the capsule wall grows inward from the surface of the template, a lumen and numerous mesopores on the capsule wall are simultaneously generated after removing the template. Specifically, PAH-segregated templates (P-$CaCO_3$ microspheres) are first synthesized through in situ entrapping PAH during the formation of $CaCO_3$ microspheres, which are then cross-linked via glutaraldehyde (GA) (forming PG-$CaCO_3$ microspheres). Subsequently, the as-synthesized PG-$CaCO_3$ microspheres are immersed into the aqueous solution of Ti (IV) bis-(ammonium lactate) dihydroxide (Ti-BALDH) to implement biomimetic mineralization (forming PGTi-$CaCO_3$ microspheres), followed by removal of $CaCO_3$ microspheres, leading to the mesoporous hybrid microcapsules (PGTi microcapsules). The chemical composition, morphologies, wall thickness, pore size, and permeability of the microcapsules can be facilely modulated. This approach offers several distinct and unique advantages. First, mesoporous hybrid microcapsules are synthesized under rather mild conditions. Second, it is widely applicable for synthesizing a variety of polymer-inorganic microcapsules from different combinations of cationic hydrophilic polymers (e.g., polylysine, polyarginine, etc.), cross-linkers (e.g., tannic acid, genipin, etc.), and inorganic precursors (e.g., silica, zirconia, etc.). Third, the resultant microcapsules can exhibit controllable permeability for different sized molecules and can be utilized in many diffusion-governed processes, such as enzymatic catalysis, wastewater treatment, drug delivery, etc.

2. EXPERIMENTAL SECTION

2.1. Materials. Poly(allylamine hydrochloride) (PAH, $M_w \approx 15$ kDa and 70 kDa), Ti(IV)-bis-(ammonium lactate) dihydroxide (Ti-BALDH, 50 wt. % aqueous solution), tris(hydroxymethyl)-amiomethane (tris), formate dehydrogenase from *Candida boidinii* (FateDH, EC.1.2.1.43), formaldehyde dehydrogenase from *Pseudomonas putida* (FaldDH, EC.1.2.1.46), reduced nicotinamide adenine dinucleotide (NADH, 98%), insulin, polystyrene sulfonate sodium (PSS, $M_w \approx 70$ kDa), fluorescein isothiocyanate (FITC), and protamine were purchased from Sigma-Aldrich Chemical Co. Calcium chloride ($CaCl_2$), sodium carbonate (Na_2CO_3), sodium hydroxide (NaOH), sodium silicate, hydrochloric acid (HCl), glutaraldehyde (GA), ethylenediaminetetraacetic acid (EDTA), sodium dihydrogen phosphate, disodium hydrogen phosphate, tannic acid (TA), Congo red (CR) and methylene blue (MB) were obtained from Guangfu

Reagent Chemicals Co. (Tianjin, China). Bovine serum albumin (BSA) was purchased from the Institute of Hematology, Chinese Academic of Medical Sciences (Tianjin, China). Water used all through experiments was prepared via a Millipore Milli-Q purification system and had a resistivity higher than 18 MΩ·cm. All other reagents were analytical grade and used without further purification. Fluorescent-labeled PAH, BSA, and enzymes were prepared using overnight incubation at room temperature of their mixtures with FITC phosphate buffer solution (PBS, 50 mM, pH 8.0, PAH or protein concentration 1 mg mL^{-1}, [dye]/[PAH or protein] = 5) followed by exhaustive dialysis (M_W cutoff 14 kDa) against PBS (50 mM, pH 7.0) for 72 h and deionized water for 48 h.[12]

2.2. Fabrication of PAH/GA-Titania (PGTi) Microcapsules. PAH-$CaCO_3$ (P-$CaCO_3$) microspheres with narrow size distribution (average diameter around 3−5 μm) were used as sacrificial templates, which were prepared according to the coprecipitation method previously described in the literature.[13]

Briefly, a certain amount of PAH (0.5 and 2 mg) was dissolved in 1 mL of 330 mM $CaCl_2$ solution in a beaker under magnetic agitation (~800 rpm), into which an equal volume of 330 mM Na_2CO_3 solution was rapidly poured at specific temperature. The mixture was vigorously stirred for 30 s. After standing for 3 min, P-$CaCO_3$ microspheres were centrifuged and washed for 3 times with deionized water to get rid of the free PAH. The template synthesizing temperature was 10, 20, or 40 °C.

Then, P-$CaCO_3$ microspheres were dispersed in 1.25 mL of GA aqueous solution (pH 6.8 ± 0.2). The GA concentrations were 0.01, 0.05, 0.10, 0.20, 0.50, 1.00, and 2.00 wt. %. After the mixture was kept in a vessel under mild agitation for a certain period of time (10, 30, 60, 120, and 240 min), centrifugation and washing with deionized water were conducted several times until the excess GA was washed away.

Next, PAH/GA-$CaCO_3$ (PG-$CaCO_3$) microspheres were then dispersed in 1 mL of Ti-BALDH aqueous solution with a certain concentration (5, 10, 50, and 100 mM, pH 7.0). After the mixture was kept in a vessel under mild agitation for 60 min, centrifugation and washing with deionized water were conducted several times until the excess Ti-BALDH was washed away.

Finally, PAH/GA-titania-$CaCO_3$ (PGTi-$CaCO_3$) microspheres were incubated in 1 mL, 50 mM EDTA solution for 5 min under shaking to obtain PGTi microcapsules, which were further washed with water and fresh EDTA solution, each for 3 times, using centrifugation (3000 rpm, 3 min). Herein, PGTi microcapsules synthesized under different conditions were denoted and presented in Supporting Information Table S1. Similarly, TA (8 mg mL^{-1}) was also utilized instead of GA to fabricate the microcapsules, and the corresponding characterizations were illustrated in Supporting Information Figure S1.

2.3. Synthesis of Mesoporous Microcapsules from Other Cross-linkers or Inorganic Precursors. PAH-$CaCO_3$ microspheres with narrow size distribution (average diameter around 3−5 μm) were used as sacrificial templates, which were prepared according to the coprecipitation method previously described in the literature.[13] Briefly, 2 mg of PAH was dissolved in 1 mL of 330 mM $CaCl_2$ solution in a beaker under magnetic agitation (~800 rpm), into which an equal volume of 330 mM Na_2CO_3 solution was rapidly poured at room temperature. The mixture was vigorously stirred for 30 s. After standing for 3 min, PAH-$CaCO_3$ microspheres were centrifuged and washed for 3 times with deionized water to get rid of the free PAH.

Then, the as-prepared PAH-$CaCO_3$ microspheres were dispersed in 1.25 mL aqueous solution of various cross-linkers (pH 7.0). The species and concentration of cross-linkers are listed as follows: GA, 0.01 wt. %; TA, 8 mg mL^{-1}. After the mixture was kept in a vessel under mild agitation for 60 min, centrifugation and washing with deionized water were conducted several times until the excess cross-linker was washed away. The synthesized microcapsules are denoted as PAH/GA-$CaCO_3$ and PAH/TA-$CaCO_3$ microspheres, respectively.

Next, the as-synthesized microspheres were then dispersed in 1 mL of silicate aqueous solution (50 mM, pH 7.0−8.0). After the mixture was kept in a vessel under mild agitation for 60 min, centrifugation and washing with deionized water were conducted several times until the excess silicate was washed away.

The obtained microspheres were incubated in 1 mL, 50 mM EDTA solution for 5 min under shaking, followed by washing with water and fresh EDTA solution, each for 3 times, using centrifugation (3000 rpm, 3 min). Finally, PAH/GA-silica and PAH/TA-silica microcapsules were acquired and characterized as shown in Supporting Information Figure S2.

2.4. Mass Transfer Property. The mass transfer property of NADH from the bulk solution to various PGTi microcapsules was investigated according to previous reports.[14] 60 μL of concentrated PGTi microcapsules solution was immersed in 10 mL of a well-stirred pH 7.0, 30 mM tris-HCl buffer solution containing NADH solutions (50 mM). All the measurements were performed at 37 °C. At designed time intervals, the NADH concentration in the bulk solution was determined by a UV/vis spectrophotometer (Hitachi U-3010) as the detector. The fraction of NADH in solution was expressed as eq 1

$$\text{fraction of NADH in solution (\%)} = \frac{C_t}{C_0} \tag{1}$$

where C_0 and C_t are the NADH concentrations in the bulk solution at time *0* and *t*, respectively (M).

According to previous reports,[14,15] the fraction of NADH in solution should be also described as eq 2

$$\text{fraction of NADH in solution (\%)} = \frac{\alpha}{1+\alpha}\left[1 + \sum_{n-1}^{\infty} \frac{6(1+\alpha)\exp(-D_m q_n^{\,2} t/R^2)}{9 + 9\alpha + q_n^{\,2}\alpha^2}\right] \tag{2}$$

where D_m was the mass transfer coefficient of microcapsules ($m^2\ s^{-1}$), *R* was the radius of a microcapsule (m), *r* was the distance from the center of a microcapsule (m), *t* was time (s), α was defined as $(V/N)(4\pi R^3/3)$, *V* was the volume of the solution excluding the space occupied by microcapsules (L, *V* was 60 μL in the present study), *N* was the number of microcapsules (*N* was 10^4 in the present study), and q_n was the nonzero positive roots of eq 3

$$\tan q_n = \frac{3q_n}{3 + \alpha q_n^{\,2}} = 0 \tag{3}$$

C_m could be obtained with the equations as described above. Then, the mass transfer coefficient of capsule wall (D_1) could be acquired on the basis of eq 4

$$D_1 = \frac{r_b - r_a}{\frac{r_b}{D_m} - \frac{r_a}{D_2}} \tag{4}$$

where r_a was the internal radius of the microcapsule (m), r_b was the external radius of the microcapsule (m), D_2 was the mass transfer coefficient in the intracapsule solution ($m^2\ s^{-1}$), which was similar to that in bulk solution (~$10^{-9}\ m^2\ s^{-1}$).

2.5. Construction of Multienzyme Systems by Using PGTi Microcapsules. To encapsulate FateDH (enzyme 1) in the lumen of the PGTi microcapsules, 1.0 mg of FateDH was added in the coprecipitation system to prepare P-$CaCO_3$ microspheres. Thereafter, these FateDH-containing P-$CaCO_3$ microspheres were used as templates to prepare FateDH-containing PG-$CaCO_3$ microspheres through GA cross-linking. To immobilize FaldDH (enzyme 2) on the capsule wall, 0.7 mg of FaldDH was added in the Ti-BALDH aqueous solution to prepare FateDH/FaldDH-containing PGTi-$CaCO_3$ microspheres. The as-synthesized microspheres were then incubated in 50 mM EDTA solution (pH 6.0, 4 °C) for 5 min under shaking to obtain the PGTi microcapsules, which were further washed with EDTA solution and water, each for 3 times, using centrifugation (3000 rpm, 3 min). Herein, the PGTi multienzyme systems were constructed based upon several PGTi microcapsules including PGTi-1, PGTi-15, and PGTi-16 microcapsules.

For comparison, two types of coimmobilized multienzyme systems were constructed. One type is named PGTi-*co* system, where two

enzymes were both encapsulated in the lumen of PGTi-1 microcapsules. The other is named PGTi-*surf* system, where two enzymes were both entrapped in the wall of PGTi-1 microcapsules. Amount of each enzyme in the two systems was equal to that in the spatially separated multienzyme systems.

2.6. Characterizations. High-resolution SEM images were recorded using a field emission scanning electron microscope (FESEM, Nanosem 430). Elemental analysis was accomplished by energy dispersive spectroscope (EDS) attached to FESEM. TEM observation was performed on a JEM-100CX II instrument. FTIR spectra of the microcapsules were obtained on a Nicolet-6700 spectrometer. Thirty-two scans were accumulated with a resolution of 4 cm^{-1} for each spectrum. Optical and fluorescence images were taken using an Olympus BX51 microscope with a 100 × oil immersion objective lens (Olympus, Tokyo, Japan). The excitation wavelength was chosen as 488 nm according to the FITC-labeled enzymes. Confocal laser scanning microscopy (CLSM) images were taken with a LSM 710 Confocal Microscope. The excitation wavelength was chosen as 488 nm according to the FITC-labeled PAH and BSA. The surface properties of microspheres were characterized by X-ray photoelectron spectroscopy (XPS) in a Perkin-Elmer PHI 1600 ESCA system with a monochromatic Mg Kα source and a charge neutralizer. The pore-size distribution of the microcapsules was determined by nitrogen adsorption−desorption isotherm measurements performed at 77 K on a Tristar 3000 gas adsorption analyzer. Pore-size distribution curves were calculated on the basis of the adsorption branch of nitrogen isotherms using the Barrett−Joyner−Halenda (BJH) method. The themo-gravimetric (TG) analysis and derivative thermo-gravimetric (DTG) analysis were performed on a themo-gravimetric analyzer (Pyris 1, Perkin-Elmer, USA), with an air flow at a rate of 100 mL min^{-1}.

2.7. Enzyme Immobilization and Enzymatic Cascade Conversion of CO_2 to Formaldehyde. Immobilization efficiency of each enzyme in PGTi microcapsules was also determined. More specifically, the immobilization efficiency for FateDH or FaldDH (%) was calculated according to eq 5 and 6:

$$\text{immobilization efficiency of FateDH \%)} = \frac{M_{\text{FateDH,immobilized}}}{M_{\text{FateDH,added}}} \quad (5)$$

$$\text{immoblization efficiency of FaldDH (\%)} = \frac{M_{\text{FaldDH,immobilized}}}{M_{\text{FaldDH,added}}} \quad (6)$$

where $M_{\text{FateDH,immobilized}}$ was the mass of immobilized FateDH (μg), $M_{\text{FaldDH,immobilized}}$ was the mass of immobilized FaldDH (μg), $M_{\text{FateDH,added}}$ was the mass of initially added FateDH (mg), and $M_{\text{FaldDH,added}}$ was the mass of initially added FateDH (mg). $M_{\text{FateDH,immobilized}}$ or $M_{\text{FaldDH,immobilized}}$ was calculated by measuring the concentration of FateDH or FaldDH in the supernatant before and after immobilization (25 ± 0.2 °C). To test the enzyme leakage property of the microcapsules, we added enzymes-containing microcapsules (FateDH in the lumen and FaldDH in the capsule wall) into 1 mL of tris-HCl (50 mM, pH 7.0), and incubated them at room temperature for a period of time followed by centrifugation. The content of FateDH or FaldDH in the supernatant was then determined by the micro-Bradford method using a UV/vis spectrophotometer (Hitachi U-3010) as the detector.

Conversion of CO_2 to formaldehyde was conducted in aqueous solution with free or immobilized enzymes. The pressure was maintained at 0.3 MPa. The formaldehyde concentration was determined by gas chromatography (GC) equipped with a flame ionization detector (FID; Hewlett-Packard, model HP-6890). All the measurements were repeated three times. It should be mentioned that the formic acid concentration was too low to be detected. Conversion of CO_2 by PGTi microcapsules was performed according to the following procedure. Briefly, 0.5 mL of PGTi microcapsules-containing PBS solution (50 mM, pH 7.0) was bubbled with CO_2 for 0.5 h before adding 0.5 mL of NADH PBS solution (50 mM, pH 7.0) to initiate the enzymatic reaction (the actual amount of encapsulated FateDH and FaldDH was 0.42 mg and 0.45 mg, respectively, with a final NADH concentration of 50 mM). By contrast, the same amount of free enzymes and enzymes coimmobilized in PGTi microcapsules had also undergone the catalytic activity evaluation. The formaldehyde yield (the enzyme units added to each multienzyme system were equal, %) was calculated based on eq 7

$$\text{formaldehyde yield (\%)} = \frac{2C_{\text{formaldehyde}}}{C_{\text{NADH,0}}} \quad (7)$$

where $C_{\text{formaldehyde}}$ was the concentration of formaldehyde after the enzymatic reaction (M), $C_{\text{NADH,0}}$ was the initial concentration of NADH (M).

2.8. Batch Adsorption Equilibrium of Water-Soluble Dyes and the Regeneration of PGTi-1 Microcapsule Adsorbents. Adsorption isotherm was acquired by adding a specified amount of the adsorbent samples (60 μL of concentrated PGTi-1 microcapsules solution, containing ~5.0 mg of PGTi-1 microcapsules in dry state) to a series of beakers containing 10 mL of diluted MB (or CR) solutions (10−100 mg L^{-1}). The pH value of the solution was maintained at 9.0 (or 7.0) by adding 100 mM NaOH or 100 mM HCl solutions. The beakers were sealed and kept at air-bath oscillator under 25 ± 0.2 °C for 24 h to reach equilibrium. The beakers were then removed from the oscillator, and the final concentration of MB (or CR) in the solution was measured at the maximum absorption wavelength of MB (665 nm) (or CR (495 nm)) by a UV/vis spectrophotometer (Hitachi U-3010) as the detector. The amount of MB (or CR) adsorbed at equilibrium, which is adsorption capacity (mg g^{-1}), was calculated using eq 8

$$\text{adsorption capacity (mg g}^{-1}) = \frac{V(C_0 - C_e)}{M} \quad (8)$$

where C_0 and C_e (mg L^{-1}) are the initial and equilibrium concentrations of MB (or CR) solution, respectively, V is the solution volume (L), and M is the mass of microcapsules (g).

The PGTi-1 microcapsules loaded with MB were incubated in 10 mL tris-HCl buffer solution with pH of 7.0. Then 1.0 mL of the supernatant was taken out each time from the system, while supplementing the same volume of buffer solution to keep the constant total volume of 10 mL. The characteristic absorbance of MB was recorded. The cumulative released amount was calculated for each measurement.

2.9. Protein Drug (Insulin) Loading and Release in Vitro. To encapsulate insulin (model protein drug) in the lumen of PGTi-1 microcapsules, 0.5 mg of insulin was added in the coprecipitation system to prepare P-$CaCO_3$ microspheres. After cross-linked by GA, the PG-$CaCO_3$ microspheres were added in the Ti-BALDH aqueous solution. The as-obtained microspheres were then incubated in with EDTA solution under shaking to obtain the insulin-containing PGTi microcapsules, which were further washed with water and fresh EDTA solution, each for 3 times, using centrifugation. Herein, it should be noted that all the synthesizing conditions of insulin-loaded PGTi-1 microcapsules were consistent with that of PGTi-1 microcapsules. UV/vis spectroscopy was employed to estimate the loading efficiency. Then, the insulin-loaded PGTi-1 microcapsules were incubated in 10 mL tris-HCl buffer solution (pH 7.0), MES buffer solution (pH 5.3), acetate buffer solution (pH 3.0), and NaOH solution (pH 11.0). Then 1.0 mL of the supernatant was taken out each time from the system, while supplementing the same volume of buffer solution to keep the constant total volume of 10 mL. The characteristic absorbance of insulin was recorded. The cumulative released amount was calculated for each measurement.

2.10. Entrapment Efficiency of PAH. The entrapment efficiency (mg g^{-1} ($CaCO_3$)) of PAH was calculated based on P-$CaCO_3$ microspheres, which was calculated according to eq 9

$$\text{entrapment efficiency of PAH (mg g}^{-1}(\text{CaCO}_3)) = \frac{M_{\text{PAH}}}{M_{\text{CaCO}_3}} \quad (9)$$

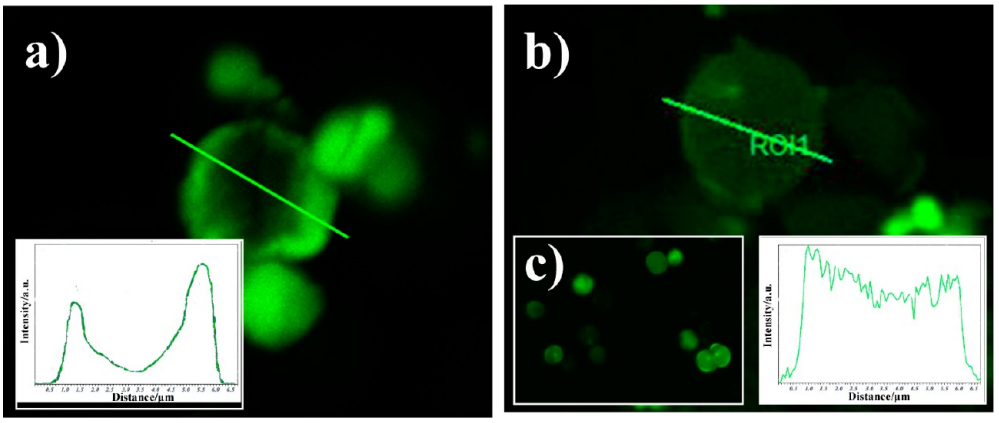

Figure 2. Caption CLSM images of the $CaCO_3$ microspheres loaded with (a) FITC-labeled PAH and (b, c) FITC-labeled BSA and the fluorescence intensity profile (inset) along the radial direction of the (a) PAH- and (b) BSA-loaded microspheres.

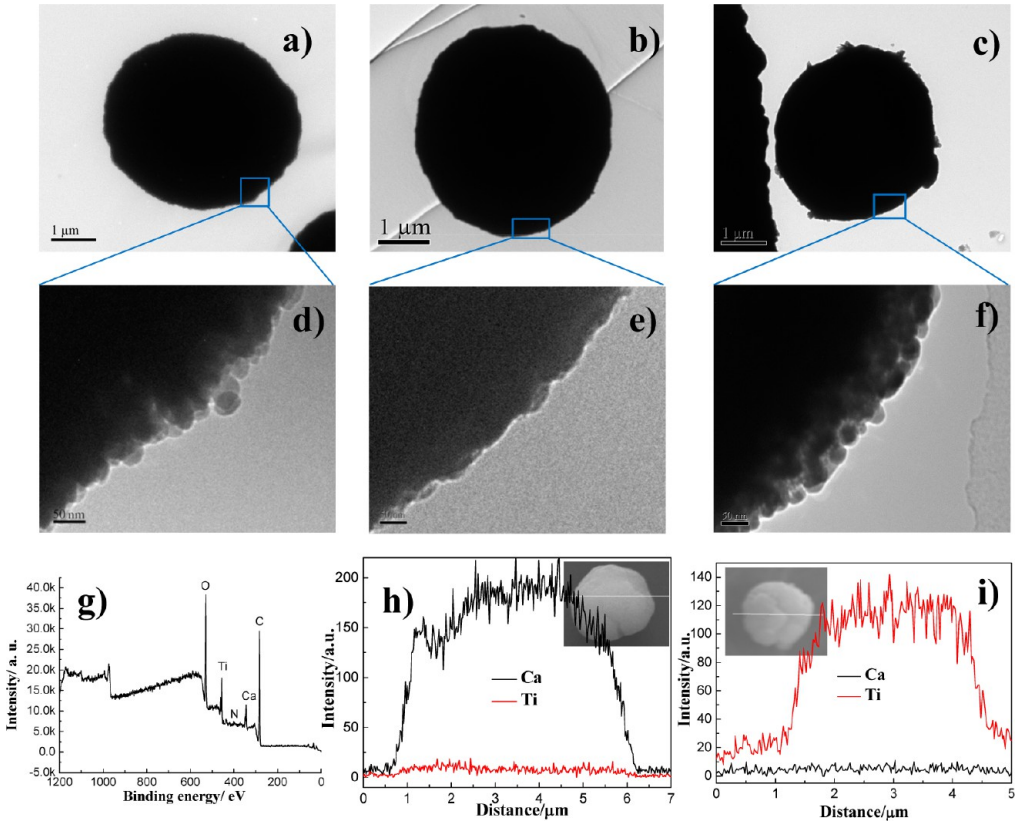

Figure 3. TEM images of (a, d) P-$CaCO_3$ microspheres, (b, e) PGTi-$CaCO_3$ microspheres, and (c, f) PGTi microcapsules. (g) XPS spectrum of PGTi-$CaCO_3$ microspheres and EDS spectra (inset, SEM images) of (h) PGTi-$CaCO_3$ microspheres and (i) PGTi microcapsules. (PAH, M_w = 70 kDa, concentration = 2 mg mL^{-1}).

where M_{PAH} was the mass of entrapped PAH (mg) and M_{CaCO_3} was the mass of pure $CaCO_3$ microspheres (g).

3. RESULTS AND DISCUSSION

3.1. Formation and Characterization of PGTi Microcapsules. Figure 1 illustrates the fabrication procedure of PGTi microcapsules. The first step is the in situ entrapment of PAH through coprecipitation of $CaCl_2$ and Na_2CO_3. As shown in the CLSM image (Figure 2a), the fluorescence emission is stronger from the near-surface region than the interior region of $CaCO_3$ microspheres, demonstrating the surface segregation of PAH. This phenomenon is in accordance with previous literature.[13] In theory, the occurrence of surface segregation is mainly driven by the decrease in Gibbs free energy of the system. It has been proven that hydrophilic or hydrophilic block-containing polymers tend to reside in the near-surface region of a water-immiscible substance, which would reduce the interfacial tension and Gibbs free energy between the hydrophobic substance and water.[16] Therefore, PAH could be spontaneously enriched in the near-surface region of $CaCO_3$ microspheres. To further explore the essential requirements for segregation process, anionic hydrophilic biopolymer (FITC-labeled BSA) is adopted as the control polymer of PAH. In the coprecipitation process of BSA and $CaCO_3$, the green fluorescent is uniformly distributed within $CaCO_3$ micro-

dx.doi.org/10.1021/am401017y | ACS Appl. Mater. Interfaces 2013, 5, 5174−5185

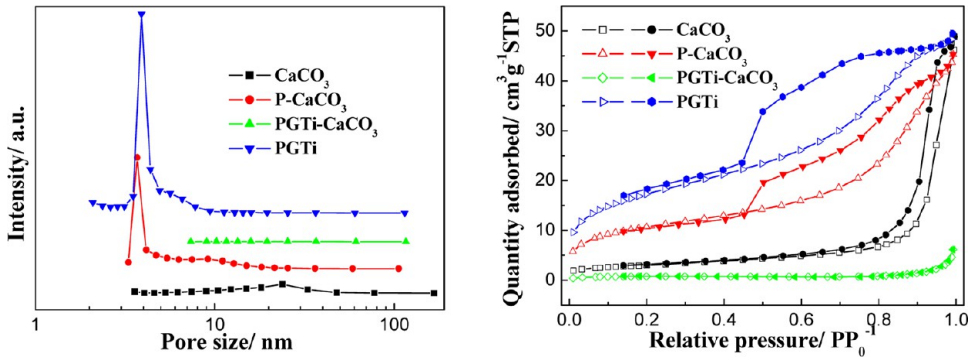

Figure 4. N_2 adsorption−desorption isotherm and the calculated pore size distribution (Barrett−Joyner−Halenda method) of (a) $CaCO_3$ microspheres, (b) P-$CaCO_3$, microspheres, (c) PGTi-$CaCO_3$ microspheres, and (d) PGTi microcapsules (PAH, M_w = 70 kDa, concentration = 2 mg mL^{-1}).

spheres without apparent segregation (Figure 2b). A possible explanation is described as follows. At neutral pH, BSA possess numerous COO^- groups, which would partly bind to Ca^{2+}.[17a,b] The formation of polymer-Ca^{2+} complex would then reduce the water solubility (hydrophilicity) of these polymers. On the contrary, Cl^- cannot be enriched around BSA molecules due to the electrostatic repulsion interaction, thus maintaining a free state. Therefore, once the BSA-containing $CaCl_2$ aqueous solution is mixed with Na_2CO_3 aqueous solution, CO_3^{2-} would be first combined with Ca^{2+} to form nano-$CaCO_3$, which has the minimum solubility product. Accordingly, BSA would be physically entrapped accompanying the formation of nano-$CaCO_3$, which resulted in a uniformly distribution of BSA within nano-$CaCO_3$ aggregations (or $CaCO_3$ microspheres). For PAH, in $CaCl_2$ aqueous solution, the existence of electrostatic repulsion between -NH_3^+ groups in polymers and Ca^{2+} would keep the NH_3^+ groups in protonated state, endowing the cationic hydrophilic polymers with high water solubility (hydrophilicity).[17c,d] Meanwhile, although PAH can attract some anions such as Cl^-, the solubility and hydrophilicity of PAH would not be affected. Therefore, once adding Na_2CO_3 to the mixture, CO_3^{2-} would be first combined with Ca^{2+} to form nano-$CaCO_3$, which has the minimum solubility product. Then, PAH would be physically entrapped through the aggregation of nano-$CaCO_3$ and trends to segregate to the water phase due to its high solubility and hydrophilicity, leading to surface segregation phenomenon. It is also worthy to mention that, because of the rather weak hydrogen bond between PAH chains, PAH has to be cross-linked to retain the intact polymer network. This cross-linked microsphere is subsequently employed to implement biomimetic mineralization of Ti-BALDH to produce titania. After removing $CaCO_3$ microspheres, numerous mesopores are generated on the capsule wall by the templating of the PAH-rich region of $CaCO_3$ microspheres, whereas capsule lumen is formed by the templating of the PAH-lean region of $CaCO_3$ microspheres. To test the universality of this approach, several kinds of mesoporous hybrid microcapsules have been prepared using different cross-linkers and inorganic precursors (Supporting Information Figure S1 and S2). In the present study, PGTi microcapsules are chosen as a representative for the subsequent characterizations and applications.

Essential characterizations (i.e., transmission electron microscopy (TEM), X-ray photoelectron spectroscopy (XPS), and energy dispersive spectroscope (EDS)) are conducted to elucidate the fabrication process of PGTi microcapsules. As shown in Figure 3a−3c, under low magnification, no apparent morphological difference could be observed among P-$CaCO_3$ microspheres, PGTi-$CaCO_3$ microspheres and PGTi microcapsules. In the high resolution-TEM images, numerous aggregated nanoparticles appear in the edge of P-$CaCO_3$ microspheres (Figure 3d). After polymer cross-linking and biomimetic mineralization, the nanoparticles could not be identified or distinguished (Figure 3e), indicating the polymer network among aggregated nanoparticles is totally filled with GA and titania. Along with the dissolution of $CaCO_3$ microspheres, mesoporous structure of PGTi microcapsules is then generated (Figure 3f). To confirm the hollow, intact structure of PGTi microcapsules, optical image is acquired as shown in Supporting Information Figure S3.

On the basis of the microcapsule formation process monitored by TEM, it can be conjectured that the capsule wall grows inward from the surface of P-$CaCO_3$ microspheres. A hollow core/lumen and numerous mesopores on the capsule wall are simultaneously generated after removing $CaCO_3$ microspheres. To check this, XPS spectrum (Figure 3g) is conducted to probe the surface chemical composition of PGTi-$CaCO_3$ microspheres. Existence of calcium element at 344.9 and 348.4 eV indicates that no continuous PAH layer is capped on the surface of PGTi-$CaCO_3$ microspheres. Besides, nitrogen element at 397.1 eV and titanium element at 456.3 and 462.1 eV originates from PAH and titania, respectively. Meanwhile, as illustrated by the EDS spectra in Figure 3h, for PGTi-$CaCO_3$ microspheres, calcium element and titanium element appear and disappear synchronously as the electron beam goes through the particle surface, which also offers a strong evidence for the inward growth of the capsule wall. After treating PGTi-$CaCO_3$ microspheres with EDTA, no calcium element can be detected (Figure 3i), indicating the complete removal of $CaCO_3$ component.

The Brunauer−Emmett−Teller (BET) results correlate well to the TEM images (Figure 4). Specifically, compared with pure $CaCO_3$ microspheres, P-$CaCO_3$ microspheres possess higher surface area (38.7 vs 10.6 m^2 g^{-1}) and more uniform pore size distribution (3.7 vs 10−50 nm). Similar to the TEM observation, quite a low surface area (2.7 m^2 g^{-1}) and porosity (0.009 cm^3 g^{-1}) of PGTi-$CaCO_3$ microspheres further verify that the polymer network is completely filled with GA and titania. After removing $CaCO_3$ microspheres, drastically enhanced surface area (62.6 m^2 g^{-1}) and porosity (0.081 cm^3 g^{-1}) are obtained for PGTi microcapsules. Primary pore size is around 4 nm as calculated by Barrett−Joyner−Halenda (BJH)

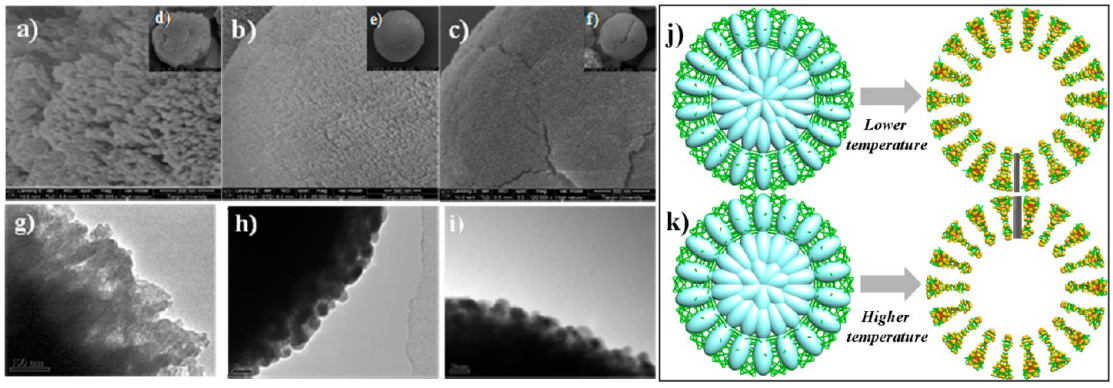

Figure 5. SEM images of P-$CaCO_3$ microspheres synthesized at (a, d) 40, (b, e) 20, and (c, f) 10 °C. TEM images of (g) PGTi-16, (h) PGTi-1, and (i) PGTi-15 microcapsules. Schematic synthesis procedure of PGTi microcapsules at (j) lower and (k) higher template synthesizing temperature (PAH, M_w = 70 kDa, concentration = 2 mg mL^{-1}).

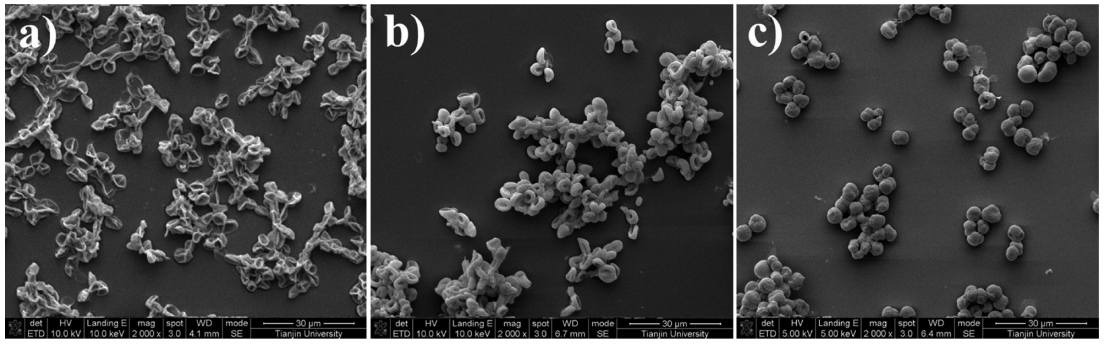

Figure 6. Morphologies of PGTi microcapsules synthesized under different conditions: (a) PAH 15 kDa, 2 mg mL^{-1}; (b) PAH 70 kDa, 0.5 mg mL^{-1}; and (c) PAH 70 kDa, 2 mg mL^{-1}. Note: All other synthetic conditions are equal, especially, the cross-linking time are all 60 min.

method. Notably, once the as-synthesized PGTi microcapsules are frozen dried, the surface area and porosity would be decreased compared with the microcapsules in wet state (the surface area and the pore volume are 71.0 m^2 g^{-1} and 0.312 cm^3 g^{-1}, respectively). The pore volume of the capsules in wet state is nearly four times higher than that of the capsules in dry state, which is comparable to that of silica mesoporous microcapsules.[18]

3.2. Morphology and Structure Control of PGTi Microcapsules. Previous reports have proved that the particle size of the $CaCO_3$ microspheres can be tuned by varying the stirring time and speed after mixing $CaCl_2$ with Na_2CO_3.[19] Increase of both stirring time and speed leads to more pronounced salt intermixing and, as a result, larger number of nuclei and smaller crystals. Besides, increase of salt concentration also causes the decrease in size of the crystals. However, for a given diameter of $CaCO_3$ microspheres, parameters affecting their microstructure (e.g., aggregated nanoparticle size, pore size, and surface area) are rarely investigated.[19] In the present study, template synthesizing temperature is changed to modulate the microstructure of $CaCO_3$ microspheres, and subsequently to control the morphological and structural characteristics of PGTi microcapsules. As demonstrated in Figure 5d−5f, the particle size keeps a constant value of ∼5 μm. Increase of synthesizing temperature renders larger aggregated nanoparticle size, larger average pore size, as well as higher surface area (Figure 5a−5c and Supporting Information Figure S5), while the porosity changes only slightly (0.071−0.080 cm^3 g^{-1}, dry state). Becaue of the structure difference among the three sacrificial P-$CaCO_3$ templates, the resultant PGTi microcapsules (Hereafter, the synthesizing conditions and mechanical strength of serious PGTi microcapsules are listed in Supporting Information Table S1.) have different morphologies and structures as shown in Figure 5g−5i. The average pore size on the capsule wall of PGTi-16 is the largest (PGTi-16, 6.7 nm; PGTi-1, 4.3 nm; PGTi-15, 3.0 nm; statistics from Figure 5g−5i of TEM images), mainly because of the larger aggregated nanoparticle size of the sacrificial P-$CaCO_3$ templates as schematically shown in Figure 5j and 5k.

As illustrated from the schematic preparation procedure of PGTi microcapsules (Figure 1), surface segregation of PAH is crucial for the generation of capsule core/lumen and mesopores on the capsule wall. Therefore, through changing the segregation conditions, the capsule morphology and the thickness of the capsule wall could be tailored. As shown in Figure 6a, PGTi microcapsule synthesized with lower-molecular-weight PAH (15 kDa) has a thinner capsule wall (∼230 nm) and a collapsed morphology. In contrast, higher-molecular-weight PAH (70 kDa) renders the microcapsule a thicker capsule wall (∼600 nm, Figure 6c) and a intact spherical morphology. As mentioned previously, both lower-molecular-weight and higher-molecular-weight PAH can migrate or segregate to the near-surface region of $CaCO_3$ microspheres during the coprecipitation process. Since the formation of $CaCO_3$ microspheres is derived from the aggregating process of numerous nanoparticles, higher-molecular-weight PAH would be more easily entrapped (with less leaching into the aqueous solution) within $CaCO_3$ microspheres than lower-molecular-weight PAH. Thus, more amount of PAH is entrapped within $CaCO_3$ microspheres which is in accordance with our

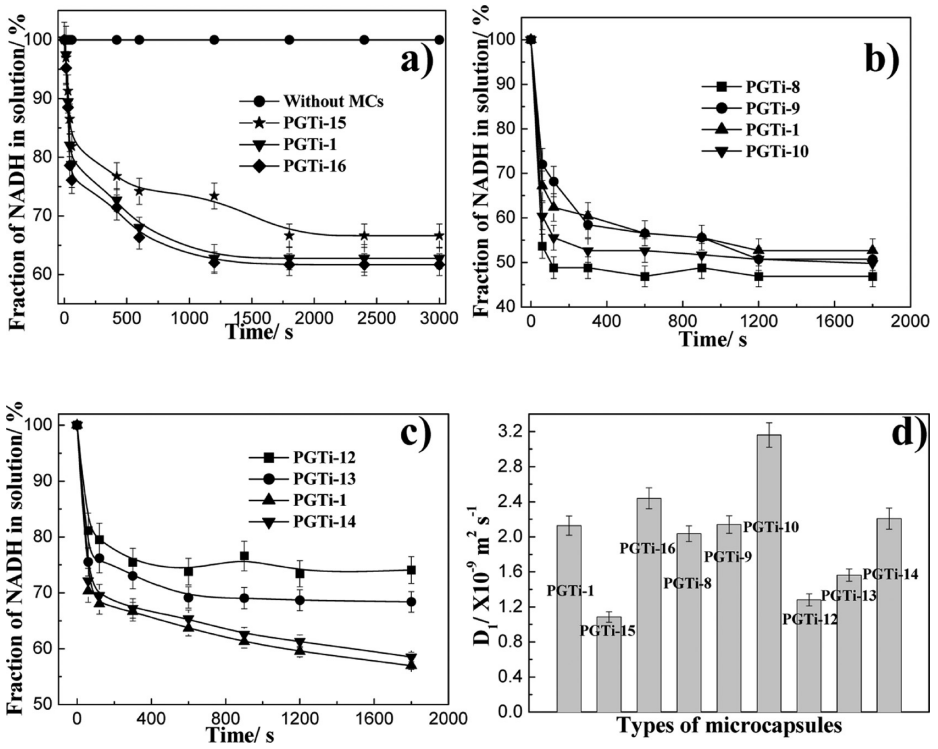

Figure 7. Mass transfer property of PGTi microcapsules as a function of (a) template synthesizing temperature, (b) cross-linking time, and (c) Ti-BALDH concentration and (d) summary of the mass transfer coefficients (D_1) of the capsule wall for different PGTi microcapsules (PAH, M_w = 70 kDa, concentration = 2 mg mL^{-1}).

experimental data. (The entrapment capacity of higher-molecular-weight PAH is 10.06 mg g^{-1} ($CaCO_3$), which is much higher than that of lower-molecular-weight PAH (4.16 mg g^{-1} ($CaCO_3$)).) Finally, thicker PAH layer could be formed in the near-surface region of $CaCO_3$ microspheres, which finally results in thicker capsule wall. In addition, for an idential molecular weight (70 kDa), PAH with a lower concentration could also result in a thinner capsule wall (*ca.* 390 nm, Figure 6b). This may be owing to the difference in entrapment capacity of PAH. Lower concentration of PAH has caused lower entrapment capacity (4.80 mg g^{-1} ($CaCO_3$) for 0.5 mg mL^{-1} vs 10.06 mg g^{-1} ($CaCO_3$) for 2.0 mg mL^{-1}), which then results in thinner PAH layer in the near-surface region of $CaCO_3$ microspheres. Finally, thinner capsule wall is acquired. Besides, the effect of other factors (*e.g.,* cross-linking time, GA concentration, Ti-BALDH concentration, etc.) on the capsule morphologies and chemical compositions has also been investigated detailedly (Supporting Information Figure S6−S9).

3.3. Mass Transfer Property of PGTi Microcapsules. Additionally, in many applications, enhancing the mass transfer rate of small guest molecules and the exposed number of active sites can greatly elevate the performance of the functional materials. Therefore, mass transfer experiments are conducted by using reduced nicotinamide adenine dinucleotide (NADH, $M_w \approx 709$ Da) as a model molecule. The mass transfer coefficient in the capsule wall for different PGTi microcapsules is calculated and summarized in Figure 7.[20] Obviously, the concentration of NADH quickly decreases to a constant value within 2000 s for all PGTi microcapsules, indicating a relatively low mass transfer resistance. The capsule wall for all PGTi microcapsules can render a mass transfer coefficient of higher than 1×10^{-9} m^2 s^{-1}, which is comparable to that in pure water ($\sim 10^{-9}$ m^2 s^{-1}). The mass transfer coefficient in the capsule wall for PGTi-1 microcapsules (2.128×10^{-9} m^2 s^{-1}) is a little lower than that for PGTi-16 (2.440×10^{-9} m^2 s^{-1}) but much higher than that for PGTi-15 (1.087×10^{-9} m^2 s^{-1}) due to the different pore size as evidenced by the TEM images (Figure 5g−5i). Higher pore size with similar porosity would render capsules higher mass transfer coefficient. Moreover, apparent difference in mass transfer coefficient could be found in PGTi-1, -8, -9, and -10, manifesting the inherent relevance of cross-linking time on the permeability. This may be due to the difference in the wall thickness of microcapsules. Interestingly, increase of Ti-BALDH concentration would lead to an enhanced mass transfer rate. The exact reason for such phenomenon is not clear at present.

3.4. Potential Applications of PGTi Microcapsules. *3.4.1. Multienzyme System Construction and Multienzyme Catalytic Reaction.* To explore the potential applications of PGTi microcapsules, a multienzyme system containing two enzymes was constructed for converting CO_2 to formaldehyde. FateDH and FaldDH are respectively immobilized through in situ encapsulation in the lumen and in situ physical entrapment within the capsule wall. Fluorescence image as illustrated in Supporting Information Figure S10b indicates that most FateDH locates in the lumen. The entrapment efficiency of FateDH is plotted in Supporting Information Figure S10a. Maximum efficiency locates at ∼55.0% as the FateDH concentration is fixed at 1.0 mg mL^{-1}. The physical entrapment of FaldDH within the capsule wall is also verified through a fluorescence microscope (Supporting Information Figure S10d). In Supporting Information Figure S10c, the entrapment efficiency decreases from 98.9% to 64.2% as the FaldDH concentration increases from 0.3 to 2.5 mg mL^{-1}. In addition, no enzyme is detected to leach from FateDH-encapsulated microcapsules and FaldDH-entrapped microcapsules into the

dx.doi.org/10.1021/am401017y | ACS Appl. Mater. Interfaces 2013, 5, 5174−5185

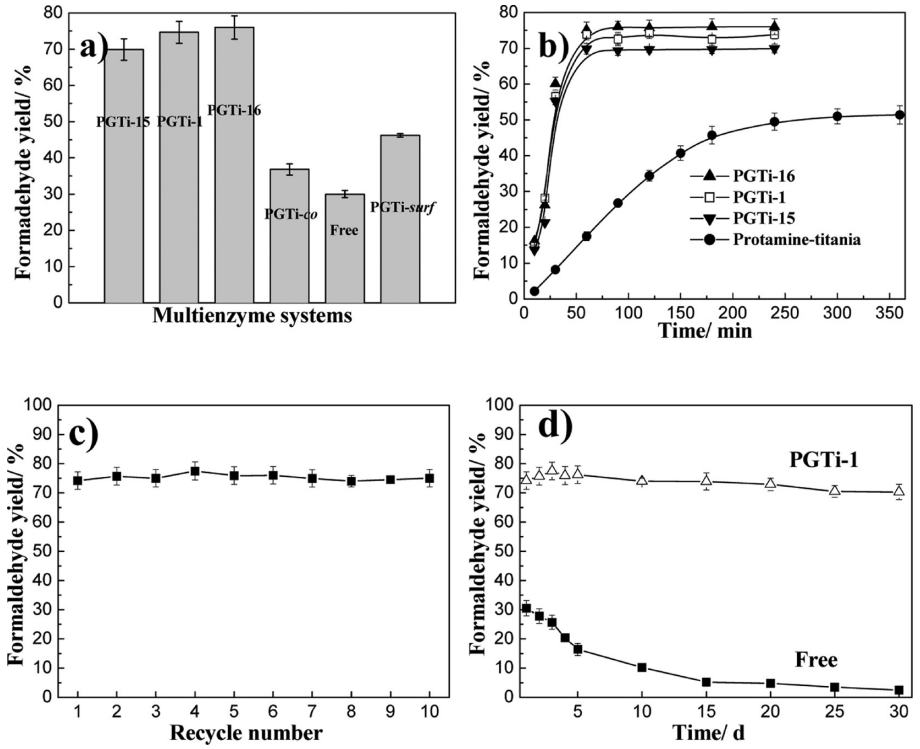

Figure 8. Plots of (a) formaldehyde yield for different multienzyme systems after reaction equilibrium, (b) formaldehyde yield of different spatially separated multienzyme systems as a function of reaction time, (c) recycling, and (d) storage stability of free and PGTi-1 systems. The reaction conditions: amount of each enzyme, FateDH/FaldDH, 0.42/0.45 mg; temperature, 37 °C; pH, 7.0 (PAH, M_w = 70 kDa, concentration = 2 mg mL^{-1}).

bulk aqueous solution during the leakage property evaluation owing to the appropriate size of mesopores (smaller than the relevant enzymes) and robust nature of PGTi microcapsules.

The conversion of CO_2 to formaldehyde involves an initial reduction of CO_2 to formic acid catalyzed by FateDH, followed by reduction of formic acid to formaldehyde by FaldDH. NADH acts as a terminal electron donor for each enzyme catalyzed reduction. As illustrated in Figure 8a, the formaldehyde yield of all the immobilized multienzyme systems (>35.0%) is higher than that of free multienzymes (30.0%). Such phenomenon could be interpreted as follows: the diffusion distance is shortened to nanometers for formic acid (the reaction intermediate) to travel between the active sites of FateDH and FaldDH. In detail, for free multienzymes, formic acid generated by FateDH has to diffuse through a longer distance to interact with FaldDH before the generation of formaldehyde. Hence, it could be deduced that the concentration of CO_2 and formic acid are low and homogeneous. For immobilized multienzyme system, an enzymatic assembly line is established. PGTi microcapsules elevate the local concentration of formic acid and confine the two enzymes in nanoscale distance. This confinement effect substantially reduces the distance for the traveling of the intermediate between the active sites of the two enzymes in comparison to free multienzymes counterpart and, thus, increases the overall rate of formaldehyde production.[21] Besides, the spatially isolated multienzyme systems convert more amount of CO_2 than coimmobilized systems as shown in Figure 8a. The tentative explanation should be that, for spatially separated multienzyme systems, CO_2 transfers through the capsule wall into the lumen and converts into formic acid thereby. The formic acid has to take a certain period to diffuse out of the lumen, which ensures that all of the formic acid molecules win sufficient time to contact with FaldDH and thus an enhanced amount of formaldehyde is produced. But for the cascade reaction catalyzed by two coimmobilizaed systems (PGTi-*co* and PGTi-*surf* systems), considerable portion of formic acid would diffuse out of the lumen without contacting with FaldDH, and the amount of formaldehyde generated is thus much lower.[22,23]

Figure 8b shows that the formaldehyde yield of all the three spatially separated multienzyme systems (PGTi-1, PGTi-15 and PGTi-16) increases almost linearly over the first 70 min, followed by a slight increase, plateauing at a nearly constant activity after 120 min. In comparison to the other two systems, PGTi-16 system exhibits the highest formaldehyde yield. The formaldehyde yield of PGTi-16 system increases from 15.0 to 76.0% as the reaction time is prolonged from 10 to 240 min. In contrast, PGTi-15 and PGTi-1 systems exhibit slightly lower activity after reaching reaction equilibrium. In particular, PGTi-15 system, of which the formaldehyde yield is ~70.0%, converts the least amount of CO_2 to formaldehyde. The formaldehyde yield (after reaction equilibrium) of PGTi-16 system are ~1.04- and 1.08-fold higher that of PGTi-1 and PGTi-15 system. Slight difference in enzymatic activity of the three microcapsules would be arisen from the different mass transfer behavior. More detailedly, since the bottleneck of the high apparent activity lies in the mass transfer property, the enhanced mass transfer coefficient for the PGTi-16 system would therefore result in a higher formaldehyde yield. To further compare the catalytic activity between porous PGTi microcapsules and conventional LbL microcapsules, protamine-titania hybrid microcapsules with nonporous capsule wall have been fabricated through LbL self-assembly and biomimetic mineralization according to

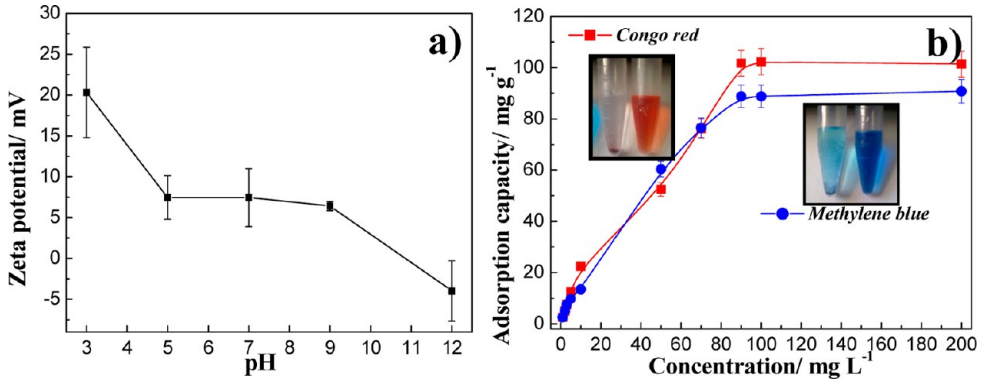

Figure 9. (a) Surface zeta potential of PGTi-1 microcapsules as a function of pH value and (b) adsorption isotherms of CR and MB on PGTi-1 microcapsules at 25 ± 0.2 °C. The pH values applied for the adsorption of CR and MB are 7.0 and 9.0, respectively (PAH, M_w = 70 kDa, concentration = 2 mg mL^{-1}).

previous report.[10c] FateDH is encapsulated in the lumen, while FaldDH is entrapped within the capsule wall. The amount of FateDH and FaldDH in the microcapsules is 0.42 and 0.45 mg, respectively. When the protamine-titania hybrid microcapsules are utilized for multienzyme catalytic reaction, and the corresponding formaldehyde yield increases much slower than that of three PGTi-based multienzyme systems (PGTi systems). Specifically, for PGTi systems, the reaction reaches equilibrium within only 70 min, along with a formaldehyde yield of higher than 70.0%. In comparison, the multienzyme system based on protamine-titania microcapsules would take ~240 min to reach reaction equilibrium with the formaldehyde yield of only 20.0%. Moreover, owing to the highly porous capsule wall, PGTi systems possess a much higher initial reaction rate (nearly 2 times) with similar formaldehyde yield in comparison to previous systems.[22,23]

For practical application, the immobilized multienzymes must be highly recyclable. Operational stability of PGTi-1 system is assessed in 10 successive batch reactions at room temperature (Figure 8c). No loss of the enzyme activity is found during the recycling because of the robust nature of the hybrid microcapsules. The storage stability of PGTi-1 system during storage at 4 °C over a 30-day period (Figure 8d) is also evaluated. This PGTi-1 system retains up to 100% of their initial activity when stored in phosphate buffer solution (PBS) for 30 days. In comparison, the formaldehyde yield of free multienzymes decreases gradually to zero with the prolongation of storing time from 0 to 30 days. These results indicate that the mesoporous hybrid microcapsules create a comfortable microenvironment for the two enzymes. According to previous reports,[23,24] the prolonged stability of these two enzymes may be partly attributed to the inherent antibiotic function from titania.

3.4.2. Wastewater Treatment. Water-soluble dyes (M_w = 300−1000 Da) is considered as a typical water pollutant. Nearly all the dye molecules have a diameter lower than 1 nm, which are commonly removed by adsorbents such as granular active carbon. The electrostatic or hydrogen bond interaction between the dyes and adsorbents plays the key role in the removal of dyes. In the present study, the adsorption capability of mesoporous hybrid PGTi-1 microcapsules is assayed. Since PGTi microcapsules are composed of PAH (a positively charged polyelectrolyte) and titania (a typical amphoteric oxide, pI ≈ 5.0), the pH value will affect the surface zeta potential of the microcapsules. In Figure 9a, PGTi-1 microcapsules possess a decreased zeta potential changing from 20.0 to −7.0 mV with the increase of pH value from 3.0 to 12.0. When the pH value is lower than 5.0, the surface zeta potential is positive. This is mainly because the pI value of PAH and titania microspheres are both greater than 5.0. When the pH value further increases, titania will donate protons rather than accepting protons, and the proton accepting ability of PAH declines. Therefore, the surface zeta potential would decrease, and finally the surface is switched into negatively charged state. Considering the porous structure and the changes of zeta potential as a function of pH value, PGTi-1 microcapsules are expected to have a high and controllable loading capability for charged molecules. Dyes molecules with different charge are employed to exploit this feature. First, Congo red (CR, M_w ≈ 696.7 Da), a negatively charged molecule, is chosen to assess the adsorption property of PGTi microcapsules. Aqueous solutions with low concentrations of CR are prepared to avoid the permeability change caused by osmotic pressure. At pH 7.0, CR can be readily adsorbed on the microcapsules owing to electrostatic attraction. And Figure 9b indicates the maximum loading capability of CR is ~99.26 mg g^{-1}(microcapsules). In comparison, also at pH 7.0, methylene blue (MB) with a smaller molecular weight (M_w ≈ 319.9 Da) but a positive charge is excluded by PGTi-1 microcapsules because of electrostatic repulsion (Supporting Information Figure S12). Increasing the pH value to regulate the surface zeta potential could facilitate the adsorption of MB on the microcapsules. And the maximum loading capability of MB is ~89.78 mg g^{-1}(microcapsules), which is 50% lower than that of granular active carbon (~200 mg g^{-1}).[26] Nevertheless, in our experiment, it is found that the dyes adsorption rate of PGTi-1 microcapsules is much faster than that of granular active carbon. To validate the rapid removal of MB by PGTi-1 microcapsules, 5 mg of microcapsules (in dry state) is added to 10 mL of MB solution with an initial concentration of 100 mg L^{-1}. The color of the solution disappeared completely within 5 min (Figure 9b and Supporting Information Figure S12), affording a direct evidence of the rapid MB adsorption on PGTi-1 microcapsules. Conversely, granular active carbon exhibited much slower adsorption rate (~400 min for color removal) because of the diffusion limitation.[25] Since the adsorption capability for MB is a function of pH value (Supporting Information Figure S12), PGTi-1 microcapsules can be facilely regenerated through incubating the MB-containing microcapsules into a neutral or acidic aqueous solution (pH < 7.0) (Supporting Information Figure S13). In a

word, the appropriate structural, physical and chemical features allow the fine-tuning of binding and release for charged dye molecules.

3.4.3. In Vitro Drug Delivery. Controlled drug delivery experiment has been also conducted in this study. Since a number of drugs, such as peptides, proteins, and oligonucleotides are with a size of 3−5 nm, release/transfer of these drugs through mesoporous materials not only depends on the nonspecific interactions (e.g., electrostatic interaction, hydrogen bond interaction, etc.) between drugs and carriers but also depends on the sieving effect. In addition, to achieve controlled drug release, carriers should possess triggered release attributes,[26] which can be used to prevent drug from leakage and deactivation during circulation and allow desired release of the therapeutics at target sites in the presence of specific physiological stimuli. In this study, pH-triggered release of insulin is investigated for PGTi-1 microcapsules. First, insulin is encapsulated in PGTi-1 microcapsules, which could obtain a loading capacity of 211 mg g^{-1}(microcapsules). These insulin-loaded microcapsules are then dispersed in buffer solutions with different pH values (Figure 10). At pH 5.3, no insulin

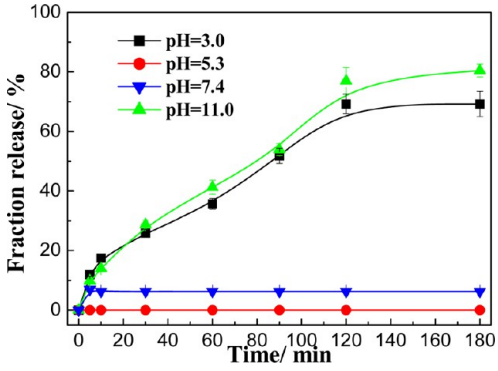

Figure 10. In vitro insulin release in PGTi-1 microcapsules as a function of pH value (PAH, M_w = 70 kDa, concentration = 2 mg mL^{-1}).

could be detected in the solution owing to the pI value of insulin being ~5.3. At such pI value, insulin is insoluble in aqueous solution. Similarly, under neutral pH, as a result of the electrostatic attraction between insulin and microcapsules, only little insulin is released to the solution. Besides, the pore size on the capsule wall would not change considerably at either pH 5.3 or 7.0, which confines insulin in the capsule lumen without significant leaking. When the pH value increases to 11.0 or decreases to 3.0, the microcapsules possess a release amount of 80.0% or 60.0%, exhibiting excellent controllable release property. The increased permeability of the microcapsules in pH 11.0 and 3.0 is due to higher charge repulsion (As shown in Supporting Information Figure S14, the zeta potentials of insulin loaded microcapsules are 25 mV (pH 3) and −10 mV (pH 11), respectively.), which enlarges the diameter of the mesopores on the capsule wall, therefore allowing the release of insulin from the microcapsules more quickly.[27]

4. CONCLUSIONS

A facile and generic approach to preparing mesoporous, hybrid microcapsules has been developed by exploring the segregating and mineralization-inducing capacities of cationic hydrophilic polymer. Specifically, $CaCO_3$ microspheres with PAH enriched in the near-surface region, is first synthesized through coprecipitation method. The microspheres are then covalently cross-linked and dipped into aqueous solution of titanium precursors to implement the biomimetic mineralization. After removing $CaCO_3$ microspheres, the mesoporous PAH-titania hybrid microcapsules are acquired. PAH plays two critical roles: (1) its hydrophilicity renders the segregating capacity and spontaneous enrichment in the near-surface region of $CaCO_3$ microspheres and (2) offering the confined space and inducing the formation of the mineralized titania. The $CaCO_3$ microspheres act as the dual templates for generating both capsule lumen and mesopores on the capsule wall. The thickness of capsule wall can be conveniently controlled by varying the surface segregation conditions and polymer cross-linking conditions, while the chemical composition, morphologies, pore size and permeability of the microcapsules can be facilely tailored through changing the template synthesizing conditions, cross-linker concentration/cross-linking time or inorganic precursor concentration. The hybrid materials render the microcapsules extremely high mechanical strength, while the mesoporous structures endow microcapsules with tunable mass transfer performance. The unique composition and mesostructure endow the microcapsules superior performance in enzyme catalysis, wastewater treatment as well as drug delivery. This study may open a novel avenue to fabricating porous hybrid microcapsules.

■ ASSOCIATED CONTENT

Ⓢ Supporting Information

Chemical structure of tannic acid (TA), SEM image and FTIR spectrum of PAH/TA-titania microcapsules, EDS spectra and SEM images of PAH/GA-silica and PAH/TA-silica microcapsules, optical image and SEM image of PGTi microcapsules, TG and DTG analysis of PGTi-$CaCO_3$ microspheres and PGTi microcapsules, N_2 adsorption−desorption isotherm of P-$CaCO_3$ microspheres as a function of synthesizing temperature, wall thickness and FTIR spectra of PGTi microcapsules as a function of cross-linking time, GA concentration, and Ti-BALDH concentration, SEM images of PGTi microcapsules incubated in GA aqueous solution with different concentrations, SEM images of PGTi microcapsules incubated in GA aqueous solution for different time, SEM images of PGTi microcapsules incubated in Ti-BALDH solution with different concentrations, encapsulation efficiency of FateDH, and entrapment efficiency of FaldDH in PGTi microcapsules, florescence image of FateDH-encapsulated PGTi microcapsules and FaldDH-entrapped PGTi microcapsules, CR adsorption capability on PGTi-1 microcapsules as a function of pH value, MB adsorption capability on PGTi-1 microcapsules as a function of pH value, release and profile of MB for PGTi-1 microcapsules as a function of time. This material is available free of charge via the Internet at http://pubs.acs.org.

■ AUTHOR INFORMATION

Corresponding Author

*E-mail: zhyjiang@tju.edu.cn. Fax: 86-22-23500086. Tel: 86-22-23500086.

Author Contributions

All authors have given approval to the final version of the manuscript.

Notes

The authors declare no competing financial interest.

■ ACKNOWLEDGMENTS

The authors thank the financial support from the National Science Fund for Distinguished Young Scholars (21125627), National Basic Research Program of China (2009CB724705), the National Science Foundation of China (20976127), and the Program of Introducing Talents of Discipline to Universities (B06006).

■ REFERENCES

(1) (a) Nudleman, E.; Wall, D.; Kaiser, D. *Science* **2005**, *309*, 125−127. (b) Braun, V. *Science* **1998**, *282*, 2202−2203.
(2) (a) Liu, J.; Liu, F.; Gao, K.; Wu, J. S.; Xue, D. F. *J. Mater. Chem.* **2009**, *19*, 6073−6084. (b) Lensen, D.; Vriezema, D. M.; van Hest, J. *Macromol. Biosci.* **2008**, *8*, 991−1005. (c) Peyratout, C. S.; Dähne, L. *Angew. Chem., Int. Ed.* **2004**, *43*, 3762−3783.
(3) Kresge, C.; Leonowicz, M.; Roth, W.; Vartuli, J.; Beck, J. *Nature* **1992**, *359*, 710−712.
(4) (a) Hoffmann, F.; Cornelius, M.; Morell, J.; Fröba, M. *Angew. Chem., Int. Ed.* **2006**, *45*, 3216−3251. (b) Wan, Y.; Zhao, D. Y. *Chem. Rev.* **2007**, *107*, 2821−2860.
(5) (a) Zeng, H. C. *J. Mater. Chem.* **2005**, *16*, 649−662. (b) Yamada, Y.; Mizutani, M.; Nakamura, T.; Yano, K. *Chem. Mater.* **2010**, *22*, 1695−1703. (c) Van Gough, D.; Wolosiuk, A.; Braun, P. V. *Nano Lett.* **2009**, *9*, 1994−1998.
(6) Wu, D.; Xu, F.; Sun, B.; Fu, R.; He, H.; Matyjaszewski, K. *Chem. Rev.* **2012**, *112*, 3959−4015.
(7) Dai, Z. F.; Dähne, L.; Möhwald, H.; Tiersch, B. *Angew. Chem., Int. Ed.* **2002**, *41*, 4019−4022.
(8) (a) He, Q.; Cui, Y.; Li, J. B. *Chem. Soc. Rev.* **2009**, *38*, 2292−2303. (b) Antipov, A. A.; Sukhorukov, G. B. *Adv. Colloid Interface Sci.* **2004**, *111*, 49−61.
(9) Feng, Z. Q.; Wang, Z. P.; Gao, C. Y.; Shen, J. C. *Adv. Mater.* **2007**, *19*, 3687−3691.
(10) (a) Caruso, F.; Caruso, R. A.; Möhwald, H. *Science* **1998**, *282*, 1111−1114. (b) Dickerson, M. B.; Sandhage, K. H.; Naik, R. R. *Chem. Rev.* **2008**, *108*, 4935−4978. (c) Jiang, Y. J.; Yang, D.; Zhang, L.; Sun, Q. Y.; Sun, X. H.; Li, J.; Jiang, Z. Y. *Adv. Funct. Mater.* **2009**, *19*, 150−156. (d) Li, J.; Jiang, Z. Y.; Wu, H.; Zhang, L.; Long, L. H.; Jiang, Y. J. *Soft Matter* **2010**, *6*, 542−550.
(11) Yang, S. H.; Lee, K. B.; Kong, B.; Kim, J. H.; Kim, H. S.; Choi, I. S. *Angew. Chem., Int. Ed.* **2009**, *48*, 9160−9163.
(12) Petrov, A. I.; Volodkin, D. V.; Sukhorukov, G. B. *Biotechnol. Prog.* **2005**, *21*, 918−925.
(13) Wang, Z. P.; Möhwald, H.; Gao, C. Y. *Langmuir* **2011**, *27*, 1286−1291.
(14) (a) Coradin, T.; Mercey, E.; Lisnard, L.; Livage, J. *Chem. Commun.* **2001**, 2496−2497. (b) Coradin, T.; Livage, J. *Mater. Sci. Eng., C* **2005**, *25*, 201−205.
(15) Zhang, L. Y.; Yao, S. J.; Guan, Y. X. *J. Chem. Eng. Data* **2003**, *48*, 864−868.
(16) (a) Yokoyama, H.; Miyamae, T.; Han, S.; Ishizone, T.; Tanaka, K.; Takahara, A.; Torikai, N. *Macromolecules* **2005**, *38*, 5180−5189. (b) Wang, Y. P.; Finlay, J. A.; Betts, D. E.; Merkel, T. J.; Luft, J. C.; Callow, M. E.; Callow, J. A.; DeSimone, J. M. *Langmuir* **2011**, *27*, 10365−10369. (d) Hester, J. F.; Banerjee, P.; Mayes, A. M. *Macromolecules* **1999**, *32*, 1643−1650.
(17) (a) Tong, W. J.; Dong, W. F.; Gao, C. Y.; Möhwald, H. *J. Phys. Chem. B* **2005**, *109*, 13159−13165. (b) Zhao, Q. H.; Zhang, S.; Tong, W. J.; Gao, C. Y.; Shen, J. C. *Eur. Polym. J.* **2006**, *42*, 3341−3351. (c) Zhao, D.; Zhuo, R. X.; Cheng, S. X. *Mol. BioSyst.* **2012**, *8*, 753−759. (d) Yu, C. Y.; Wei, H.; Zhang, Q.; Zhang, X. Z.; Cheng, S. X.; Zhuo, R. X. *J. Phys. Chem. B* **2009**, *113*, 14839−14843.
(18) Qi, G.; Wang, Y.; Estevez, L.; Switzer, A. K.; Duan, X.; Yang, X.; Giannelis, E. P. *Chem. Mater.* **2010**, *22*, 2693−2695.
(19) Volodkin, D. V.; Schmidt, S.; Fernandes, P.; Larionova, N. I.; Sukhorukov, G. B.; Duschl, C.; Möhwald, H.; von Klitzing, R. *Adv. Funct. Mater.* **2012**, *22*, 1914−1922.
(20) (a) Yao, S. J.; Guan, Y. X.; Lin, D. Q. *Ind. Eng. Chem. Res.* **2006**, *45*, 1811−1816. (b) Krediet, R. T.; Boeschoten, E. W.; Zuyderhoudt, F. M. J.; Arisz, L. *Periton. Dialysis Int.* **1986**, *6*, 61−65.
(21) Shi, J. F.; Zhang, L.; Jiang, Z. Y. *ACS Appl. Mater. Interfaces* **2011**, *3*, 881−889.
(22) (a) Obert, R.; Dave, B. C. *J. Am. Chem. Soc.* **1999**, *121*, 12192−12193. (b) El-Zahab, B.; Donnelly, D.; Wang, P. *Biotechnol. Bioeng.* **2008**, *99*, 508−514.
(23) Shi, J. F.; Wang, X. L.; Jiang, Z. Y.; Liang, Y. P.; Zhu, Y. Y.; Zhang, C. H. *Bioresour. Technol.* **2012**, *118*, 359−366.
(24) Luckarift, H. R.; Dickerson, M. B.; Sandhage, K. H.; Spain, J. C. *Small* **2006**, *2*, 640−643.
(25) Liang, H. W.; Cao, X.; Zhang, W. J.; Lin, H. T.; Zhou, F.; Chen, L. F.; Yu, S. H. *Adv. Funct. Mater.* **2011**, *21*, 3851−3858.
(26) (a) Stuart, M. A. C.; Huck, W. T. S.; Genzer, J.; Müller, M.; Ober, C.; Stamm, M.; Sukhorukov, G. B.; Szleifer, I.; Tsukruk, V. V.; Urban, M. *Nat. Mater.* **2010**, *9*, 101−113. (b) Johnston, A. P. R.; Such, G. K.; Caruso, F. *Angew. Chem., Int. Ed.* **2010**, *49*, 2664−2666. (c) Fox, M. E.; Szoka, F. C.; Fréchet, J. M. *J. Acc. Chem. Res.* **2009**, *42*, 1141−1151.
(27) Wang, A. H.; Cui, Y.; Li, J. B.; van Hest, J. *Adv. Funct. Mater.* **2012**, *22*, 2673−2681.